ACS APPLIED MATERIALS & INTERFACES

Research Article

www.acsami.org

Effect of ZnO Nanoparticle Properties on Dye-Sensitized Solar Cell Performance

Ka Kan Wong,[†] Annie Ng,[†] Xin Yi Chen,[†] Yip Hang Ng,[†] Yu Hang Leung,[†] Kam Hong Ho,[†] Aleksandra B. Djurišić,*[,†] Alan Man Ching Ng,[†,‡] Wai Kin Chan,[§] Lihong Yu,[§] and David Lee Phillips[§]

[†]Department of Physics and [§]Department of Chemistry, The University of Hong Kong, Pokfulam Road, Hong Kong

[‡]Nanostructure Institute for Energy and Environmental Research, Division of Physical Sciences, South University of Science and Technology of China, Shenzhen, China

Supporting Information

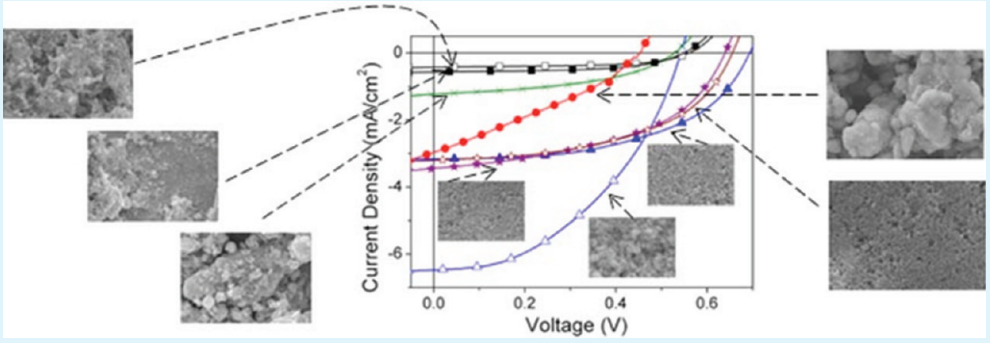

ABSTRACT: We have investigated the effect of ZnO nanoparticle properties on the dye-sensitized solar cell performance. Nanoparticles with different sizes and optical properties were considered. We found that there is a complex relationship between native defects, dye adsorption, charge transport and solar cell performance. The presence of a high concentration of nonradiative defects was found to be detrimental to photovoltaic performance, whereas for radiative defects, samples displaying orange-red defect emission exhibited better performance compared to samples with green defect emission (when the samples had similar emission intensities). Detailed discussion of the nanoparticle properties and their relationship with dye adsorption, electron injection, electron lifetime, electron transport time, and solar cell performance is given.

KEYWORDS: *DSSC, ZnO, nanoparticles, photoluminescence, defects, photovoltaics*

1. INTRODUCTION

ZnO is a wide band gap semiconductor that is of interest for applications in a wide variety of optoelectronic devices, including dye-sensitized organic solar cells (DSSCs).[1−23] Depending on the preparation method for ZnO nanostructures, different morphologies and material properties can be obtained. Various morphologies have been used in DSSCs, such as nanocrystals/nanoparticles,[1,3,5,7,8,11,15] nanodendrite/nanoparticle composites,[2] nanoporous films,[3] nanowires,[4,6,12,14,16] nanosheets,[4] nanowire/nanoparticle composites,[6] tetrapods,[8] nanorods,[9−11] nanospheres,[11,13] etc. However, the power conversion efficiencies obtained in ZnO-based DSSCs are typically significantly lower compared to TiO_2-based ones.[7] Recently, reported efficiencies exceeding 5%[18,20] are among the highest reported for ZnO, but are still significantly lower compared to TiO_2. Also, efficiencies at ∼1% or below are still commonly reported.[19] The lower efficiency of ZnO compared to TiO_2 occurs in spite of the similarities in their band structure,[7] and it can be partly explained by the dissolution of ZnO and the formation of dye−Zn^{2+} aggregates[5,7] lower injection efficiency,[5,7] lower dye regeneration efficiency,[7] and increased surface trap density after the dye adsorption.[22] Nevertheless, ZnO has a higher electron mobility compared to TiO_2.[1,7] Consequently, there is considerable interest in improving the electron transport in DSSCs by using ZnO nanostructured electrodes with various morphologies.

A considerable amount of work has been done on modifying the ZnO layer morphology in order to improve DSSC efficiency.[2,3,16] In particular, these morphology investigations have been focused on improving the surface area while at the same time enhancing the charge collection by providing faster electron transport, for example in nanowire/nanoparticle composite cells.[6,12,17] The improvements in performance with the improvements in morphology have been attributed to the fast electron transport,[17,23] higher dye loading,[17,23] and increased electron lifetime.[18] However, the performance dependence on these factors is likely complex, since it has been shown that higher efficiency can be obtained for shorter electron lifetime if

Received: October 17, 2011
Accepted: February 9, 2012
Published: February 9, 2012

Table 1. Summary of ZnO Nanoparticle Properties

				XPS					
sample[a]	purity (%)	APS (nm)	aggre. size (nm)[c]	C1s (%)	O1s (%)	Zn2p3 (%)	Zn/O_1	O_1/O_2	BET (m^2/g)
ZnO-1[1]	99.5	20	189[b], 710	4.65	48.65	46.70	1.38	1.70	45.9[c]
ZnO-2[1]	99.9	90−200	304[b], 1200	12.46	48.10	39.43	1.14	1.81	7.0[c]
ZnO-3[2]	99.9	20	2314	4.47	48.82	46.71	1.53	1.23	60.7[c]
ZnO-4[3]	99+	<10	649	4.15	47.22	48.62	1.57	1.42	30.1
ZnO-5[4]	99+	14	657	8.66	50.91	40.43	2.78	0.33	17.4
ZnO-6[4]	99+	25	892	6.26	47.04	46.70	1.69	1.08	26.4
ZnO-7[5]	99+	35−45	254, 654[b]	6.00	47.48	46.52	1.13	8.07	15.2
ZnO-8[6]	99.8	10−30	210,[b] 648[b]	4.07	48.85	47.08	1.32	1.94	13.2

[a]Superscripts denote the supplier of nanoparticles, 1 is Nanostructured & Amorphous Materials, Inc.; 2 is MKnano division, M K impex. Corp., 3 is NanoScale Corp. 4 is PlasmaChem GmbH, 5 is US Research Nanomaterials, Inc., and 6 is SkySpring Nanomaterials, Inc. [b]Majority size (if both peaks are labeled, comparable). [c]Data from ref 24.

the electron transport time is shorter,[21] or if the injection efficiency and dye regeneration efficiency are higher.[7] An improved understanding of such complex relationships would be difficult to achieve simply by improving the morphology of ZnO. Although the optimization of the morphology enhances the performance of ZnO-based DSSCs, the performance will also obviously be affected by the ZnO material properties (defect types and concentrations, charge transport within ZnO). Yet, in spite of the importance of the ZnO properties for device performance, studies on the relationship between the ZnO nanostructure properties and the corresponding solar cell performance have been scarce.[9,10]

We have investigated the solar cell performance of DSSCs based on commercial ZnO nanoparticles from different suppliers and/or with different average particle sizes (APS). These eight types of nanoparticles exhibited significantly different optical properties, dye adsorption and solar cell performance. Nanoparticles exhibit clear clustering into two groups − one group with low photoluminescence emission intensity (indicating a higher concentration of nonradiative defects) which also have significantly lower efficiency, and another group with a higher photoluminescence intensity and a higher efficiency. However, the relationship between the PL intensity and efficiency is not simple, i.e. the highest PL intensity does not imply the highest efficiency. The presence of defects responsible for orange-red emission is associated with higher short circuit current density, but lower open circuit voltage. The relationships between defects and dye injection, electron transport, and electron lifetime appear complex. It is well-known that for an optimal performance it is necessary to have high dye adsorption, long electron lifetime, and short electron transport time. However, neither one of these factors is sufficient on its own to result in high efficiency. The reasons for the observed differences in the performance of the DSSCs made with different ZnO nanoparticles and the relationship between particle properties and cell performance are discussed in detail.

It should be noted that our objective is to investigate the influence of native defects on the ZnO nanoparticles on DSSC performance. Experimental conditions have thus been kept the same for all the particles, rather than independently optimized to yield the best possible performance. The maximum achievable efficiencies would be higher with the optimization of layer thickness, dye loading time, and the introduction of a scattering layer.

2. EXPERIMENTAL SECTION

Materials and ZnO Film Preparation. Eight nanoparticles with different properties were purchased from 6 different suppliers. Particle labels and the relevant properties are summarized in Table 1. Nominal average particle size (APS) was verified by transmission electron microscopy, and the Brunauer−Emmett−Teller (BET) surface area of the samples was determined using Micromeritics ASAP 2020 surface area and porosity analyzer[24] and Quantachrome Instruments nova surface area analyzer. The obtained BET surface areas are listed in Table 1. The aggregation sizes of nanoparticles in the RO water were determined using ZETASIZER 3000HSA from Malvern Instruments Ltd.

Each of the solar cells examined here contained an active layer prepared from commercial ZnO nanoparticles listed in Table 1. For the active layer paste,[25] two kinds of pure ethyl cellulose (EC, Sigma-Aldrich) powders weighting 0.45 g in total (55 wt % of EC with viscosity 5−15 mPas and 45 wt % of EC with viscosity 30−50 mPas), were mixed with 0.5 g of ZnO nanoparticles and 3.6 g of α-terpineol (anhydrous, 90%, Sigma-Aldrich). This mixture was then sonicated and stirred by hand.

For the film preparation, the active layer was coated by screen-printing the active layer paste on FTO glass substrates (Nippon Sheet Glass, resistance 14 ohm/sq), followed by drying for 10 min at 180 °C in an oven. This procedure was repeated to obtain a sufficient thickness of the active layer. The number of repetitions for screen printing was the same for all the particles, but the active layer thickness was different because of differences in paste viscosity. Finally, the substrates were annealed at 400 °C in the furnace with a ramping rate of 1 °C/min for 3 h.

Dye-Sensitized Solar Cell Fabrication. The substrates were immersed into 0.5 mM solution of rhutenium dye N719 dye (Eversolar, Everlight Chemical Industrial Corporation, lot number D4001511) in acetonitrile (>99.9% BDH Prolabo), which was kept at 80 °C for 30 min. Afterward, the samples were rinsed by acetonitrile and dried gently. To prepare the counter electrode, a pair of holes were drilled in the Pt-coated test cell glass plate (3.2 mm thickness, TEC 15, Dyesol) for electrolyte infiltration. A solution of 0.5 M 4-tertbutpyridine (>98%, Fluka), 0.5 M Lithium iodine (LiI) (>98%, Fluka) and 0.05 M Iodine (I_2) (99.8%, Riedel-de Haen) in a mixture with 3-methoxypropionitrile solvent (>99%, Fluka) was used for the electrolyte.[9] The dye-loaded ZnO electrode and the Pt-counter electrode were assembled into a DSSC using a spacing layer of 25 μm thickness (SX1170−25, Solaronix)[9] and a hot press at 100 °C for 3 min. The electrolyte was infiltrated into the cell and then the holes were sealed using the hot-melt sealing foil and a cover glass.

Characterization. The morphology and thickness of the layers were examined by scanning electron microscopy (SEM) using a JEOL JSM-7001F SEM instrument. X-ray photoelectron spectroscopy (XPS) has been performed using Physical Electronics PHI 5600 XPS system. Photoluminescence (PL) measurements of the ZnO active layers prepared from different nanoparticles were performed using a HeCd (325 nm) laser as an excitation source, and the spectra were collected

using a PDA-512USB (Control Development Inc.) fiberoptic spectrometer. For DSSC performance characterization, a Keithley 2400 source meter was employed to measure the I−V curve in the dark and under illumination. An ABET Technologies SUN 2000 solar simulator with an AM 1.5 filter was used as a light source. The active area of the device was masked to a circle with 4 mm diameter and the power density was 100 mW/cm^2. The I−V measurements were performed under ambient conditions. Incident photon to current conversion efficiency (IPCE) measurement was carried out immediately after *I*−*V* measurement using a Oriel 66002 solar simulator with a Thermo Oriel cornerstone monochromator, a Keithley 2400 sourcemeter, and a Newport 1830-C power meter with an 818-UV detector probe.

To analyze the amount of the dye adsorbed, the samples with fixed area after dye loading were rinsed in acetonitrile to remove residual dye on the nanoparticle paste and then immersed into 0.1 mM KOH solution (pH ∼9) for at least 3 h to completely desorb and fully deprotonate the dye.[9] The absorption measurements were performed using a Cary 50 Bio 40 UV/vis spectrometer. To investigate the electron injection kinetics, fluorescence decay profiles were measured.[26] Although the injection kinetics can be studied more precisely using transient absorption spectroscopy,[27,28] because of our present equipment limitations we have not been able to perform those measurements yet and this needs further study. For fluorescence decay measurements, thin films of different ZnO nanoparticles were screen-printed on FTO/glass substrates. The nanoparticle films were than sensitized by a drop of 0.5 mM N719 solution in acetonitrile, followed by rinsing and drying. The thin film was wetted by a drop of the electrolyte solution right before the TRPL measurement. The excitation wavelength of the measurement was 403 nm to avoid any light emission from ZnO, whereas the collection wavelengths were >520 nm. Transient fluorescence decay measurements were performed by using the time correlated single-photon counting (TCSPC) technique with a confocal fluorescence microscope system (HORIBA, Ltd.). The excitation light source was a mode-locked Ar^+ ion laser. To further investigate the performance of the electron transport in the different types of ZnO samples, electrochemical impedance spectroscopy (EIS)[21,29−35] and photovoltaic transient measurements[36−39] have been performed. The electron lifetime τ_e and transport time τ_{trans} have been determined by single exponential decay fitting of photovoltage and photocurrent transients, respectively.[36,37] The EIS measurements were performed using a CH Instruments electrochemical workstation, under open circuit conditions and AM1.5 illumination.[21,29] The EIS measurements were also performed in the dark with cells biased with V_{oc} value. The values obtained from the two EIS measurements exhibited same trends. The impedance spectra obtained from the experiments were then fitted to a suitable equivalent circuit.[21] The V_{oc} transients were measured by a Keithley 238 source meter, while the cells were illuminated by a white bias light (using an Oriel 66002 solar simulator) and the light pulses from a red light emitting diode (∼625 nm, biased by a Stanford Research Systems DS345 function generator, at a frequency of 0.1 Hz). The intensity of the white bias light was tuned to make the cell voltage close to the V_{oc} value obtained from photovoltaic measurement (*J*−*V*) curves under AM 1.5 simulated solar illumination. The intensity of the red light was adjusted so that voltage increment was below 10 mV to ensure that the perturbation is small.[38] Under such conditions, i.e., small perturbation of the electron density, the electron lifetime can be determined by fitting the V_{oc} transient with an exponential decay curve.[39]

3. RESULTS AND DISCUSSION

Figures 1 and 2 show the SEM images of the active layers prepared using different ZnO nanoparticles. It can be observed that in all cases porous layers are obtained, but in the case of ZnO-3, ZnO-4, ZnO-5, and ZnO-6 significant aggregation can be observed. During annealing, there is a formation of new chemical bonds and conversion of van der Waals bonds to chemical bonds between the particles.[40] Also, in ZnO reactions between native defects and water vapor can occur even at room

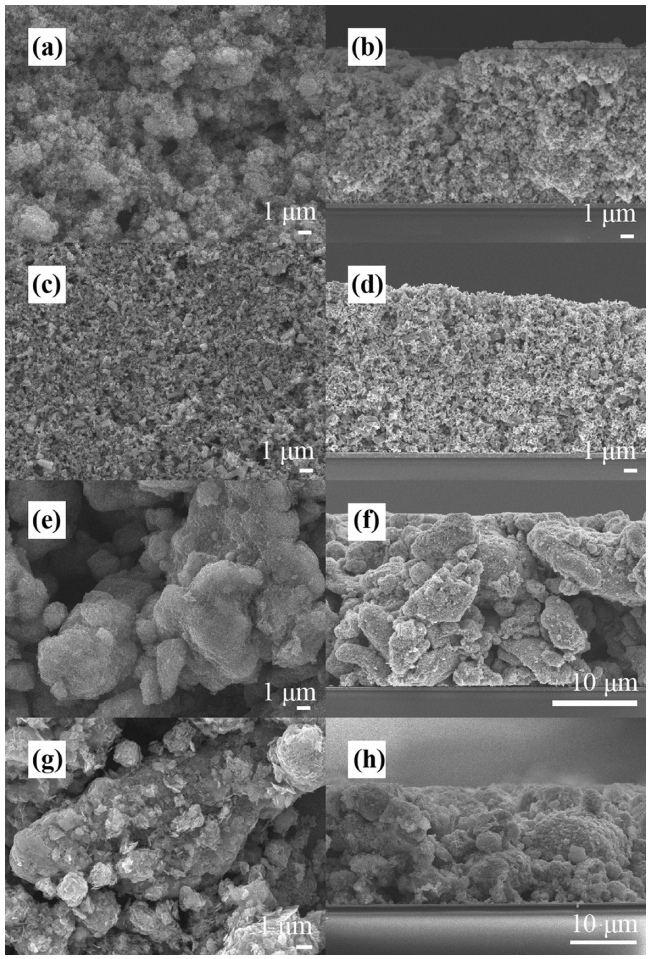

Figure 1. SEM images (top view, left; cross-section view, right) of different active layers; (a, b) ZnO-1, (c, d) ZnO-2, (e, f) ZnO-3, (g, h) ZnO-4.

temperature, resulting in nanocrystal growth and an improvement in crystallinity.[41] Thus, we would expect higher aggregation to occur in nanoparticles containing more surface defects. Similar trends are observed for aggregation sizes of different nanoparticles in water, as summarized in Table 1.

To investigate the compositions and the presence of defects in the samples, XPS and PL measurements were performed. XPS measurements provide information about the composition of the samples and to some degree on the defects (stoichiometry), whereas PL measurements allow estimates of nonradiative defects (a weaker emission implies a higher nonradiative defect concentration for identical experimental conditions), as well as different radiative defects. Concerning the composition, the samples exhibited very different ratios of zinc to oxygen, as shown in Table 1, and different shapes of the oxygen peak (see the Supporting Information, Figure S2). The oxygen peak could be fitted with two peaks (a lower energy peak O_1 corresponds to lattice oxygen,[42,43] whereas a higher energy O_2 peak is due to loosely bound oxygen on the surface, such as OH groups[42,43] or O_2^- ions in oxygen deficient regions[42]) for all of the samples except ZnO-7, where an additional contribution at ∼533 eV due to H_2O[43] can be observed. We can find that particles ZnO-3, ZnO-4, ZnO-5, and ZnO-6 generally have lower O_1/O_2 ratios. In terms of the optical properties, these four samples exhibit distinctly weaker luminescence compared to the remaining four particles: ZnO-1, ZnO-2, ZnO-7, and

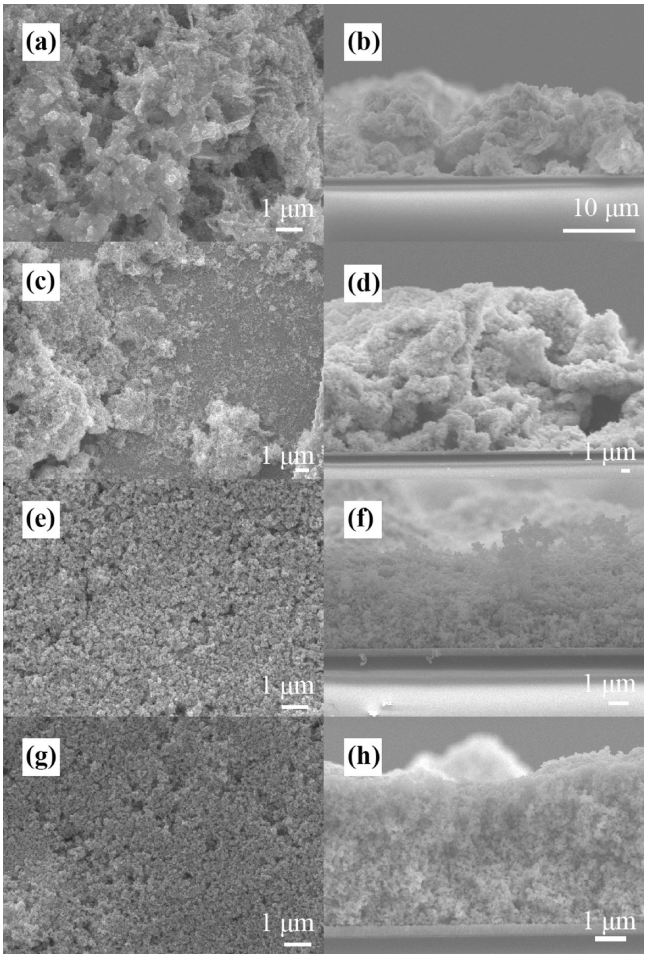

Figure 2. SEM images (top view, left; cross-section view, right) of different active layers; (a, b) ZnO-5, (c, d) ZnO-6, (e, f) ZnO-7, (g, h) ZnO-8.

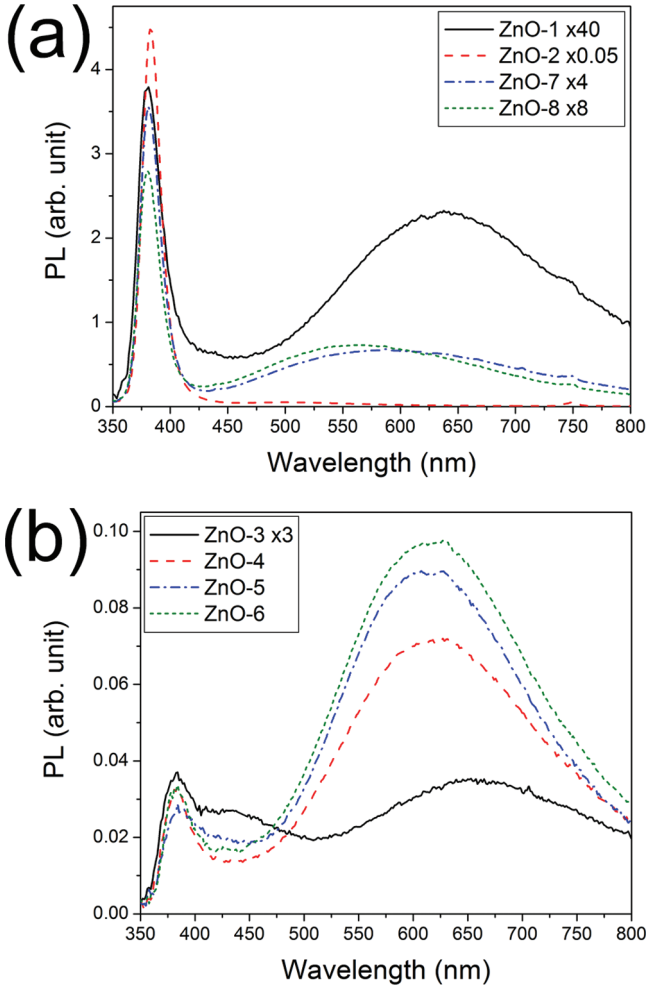

Figure 3. PL spectra of different ZnO nanoparticle active layer coatings.

ZnO-8, as shown in Figure 3. The active layers exhibit similar trends in the luminescence compared to the starting nanoparticles, despite the fact that the layer have been subjected to annealing at an elevated temperature. Annealing up to 600 °C does not result in a significant improvement of the UV-to-visible emission ratio (see the Supporting Information, Figure S1). Two of the particles, ZnO-1 and ZnO-3 exhibit orange-red defect emission, whereas the remaining nanoparticles exhibit green defect emission. Sample ZnO-2 has very low defect emission and very strong UV emission. The origin of the different defect emission bands in ZnO is still controversial.[44,45] Both the orange-red and the green emission likely originate from defect complexes, but the type of defects participating in these two emissions are likely different.[44,45] Furthermore, surface adsorbates, such as OH groups, may be involved in the orange emission from ZnO nanostructures.[45] The defect complex hypothesis is also supported by the fact that there is no clear relationship between intensities of the orange-red and green emission and XPS data, and trends between defect emissions and annealing conditions. The only clear correlation appears to be lower O_1/O_2 ratios for ZnO-3, ZnO-4, ZnO-5, and ZnO-6, which also exhibit a low intensity of the PL emission and significant aggregation. Thus, it is possible that these samples likely contain nonradiative surface defects.

We have previously shown that annealing ZnO nanorods changes their optical properties, dye adsorption and DSSC performance, but there was a complex relationship between photoluminescence and DSSC performance.[9] Here we have examined more closely the relationship between the ZnO nanoparticle optical properties, dye adsorption, and DSSC performance. The *I*−*V* and IPCE curves of the DSSCs prepared with different particles are shown in Figure 4, and the solar cell performance is summarized in Table 2. IPCE curves follow the trends of short circuit current density obtained from *I*−*V* curve measurements. Active layer thickness determined as an average of 6 points measured in cross-section SEM images is also given in Table 2, whereas absorption spectra of the desorbed dye are shown in Figure 5. Different film thickness is a consequence of different paste viscosity, due to different nanoparticle properties. When we take into account film thickness differences, the amount of dye loading is as follows: ZnO-5 > ZnO-6 > ZnO-7 > ZnO-1 > ZnO-8,ZnO-4 > ZnO-3 > ZnO-2. It can be observed that the solar cell performance trends do not match the dye loading trends, and the dye loading trends do not match the BET surface area of the nanoparticles. Native defects obviously affect the dye loading in agreement with our previous study,[9] but this relationship is complex. In terms of photovoltaic performance, we can observe that the samples with lower PL emission intensity (ZnO-3,4,5,6) exhibit inferior performance compared to samples with stronger PL emission intensity (ZnO-1,2,7,8). Also, for samples with comparable PL emission intensity, those exhibiting orange-red defect emission have

dx.doi.org/10.1021/am201424d | ACS Appl. Mater. Interfaces 2012, 4, 1254−1261

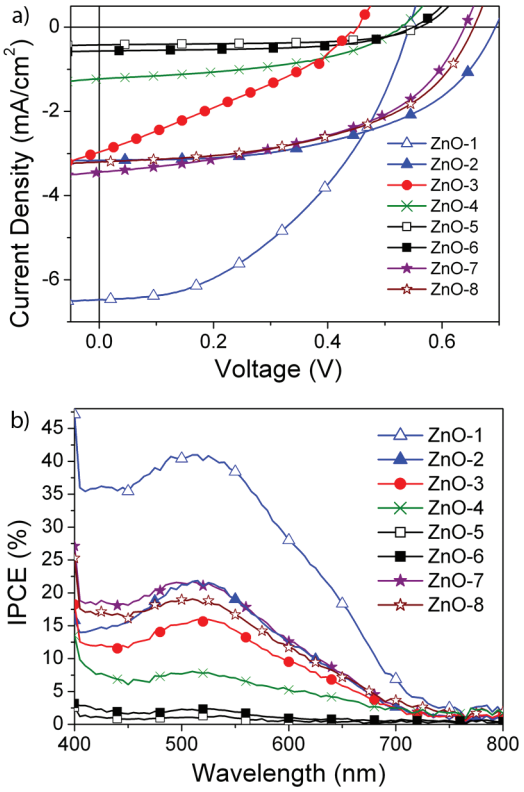

Figure 4. (a) $J-V$ curves of DSSCs prepared using different ZnO nanoparticles for the active layer. (b) IPCE curves of DSSCs prepared using different ZnO nanoparticles for the active layer.

higher short circuit current density J_{sc}, but lower open circuit voltage V_{oc} and fill factor FF compared to those exhibiting green defect emission. This is consistent with our previous study, where we observed better performance for hydrothermally grown ZnO nanorods (orange-red emission) compared to green emitting vapor-deposited ZnO nanorods (green emitting).[9] A higher surface trap density could also result in a lower fill factor of a DSSC.[22] Because we observe orange-red emission, which is not typically associated with surface defects in the samples exhibiting lower fill factors, likely these defects coexist with nonradiative surface defects, which may be responsible for the lower fill factors. This is also supported by the fact that in both groups of particles, the samples emitting in orange-red spectral region have the lowest emission intensity. Generally, the main distinguishing feature of orange-red and green defect emissions is that the green emission likely originates from the surface defects.[44] Presence of surface defects could affect the surface band bending and consequently charge injection and recombination dynamics. However, no

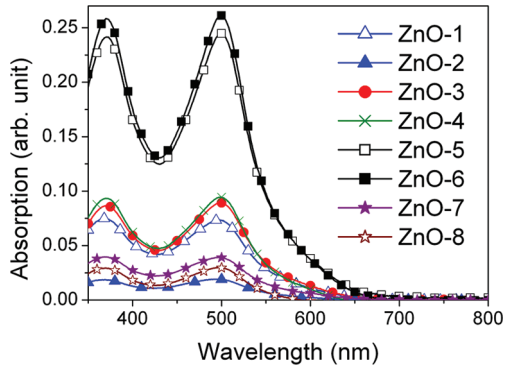

Figure 5. Absorption spectra of dye solutions desorbed from different ZnO nanoparticle active layer coatings.

clear trends are observable from fluorescence decay curves of the N719 dye on the different nanoparticles shown in Figure 6.

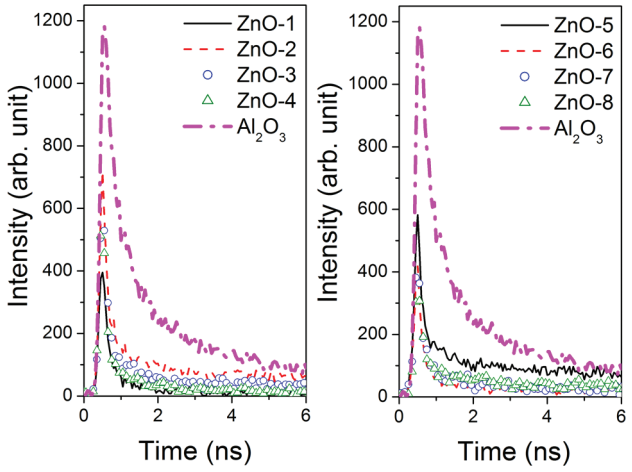

Figure 6. Fluorescence decay profiles of N719 adsorbed on different ZnO nanoparticles in electrolyte. Different nanoparticles have been separated into different figure panels (left and right) to improve clarity. A curve corresponding to Al_2O_3 as a control sample is also shown.

We can clearly see that efficient electron transfer occurs for ZnO-1 nanoparticles, but it is comparable for ZnO-3 and ZnO-4, which have different optical properties. This indicates that there is a complex relationship between electron injection and native defects in the samples, since surface defects can include both nonradiative defects and defects responsible for the green emission.

To further clarify the relationship between the photovoltaic performance and the nanoparticle properties, we performed EIS

Table 2. Summary of Device Performances for Different ZnO Nanoparticle Active Layers[a]

sample	d (μm)	V_{oc} (V)	J_{sc} (mA/cm^2)	fill factor	η(%)
ZnO-1	11.6	0.56 ± 0.01	6.1 ± 0.4 (5.9)	0.44 ± 0.01	1.5 ± 0.1
ZnO-2	11.3	0.68 ± 0.04	3.1 ± 0.2 (2.7)	0.50 ± 0.05	1.1 ± 0.1
ZnO-3	20.1	0.46 ± 0.02	2.6 ± 0.3 (2.1)	0.32 ± 0.02	0.38 ± 0.03
ZnO-4	17.5	0.54 ± 0.03	1.3 ± 0.2 (1.2)	0.45 ± 0.03	0.31 ± 0.04
ZnO-5	11.7	0.55 ± 0.02	0.4 ± 0.1 (0.2)	0.57 ± 0.02	0.12 ± 0.03
ZnO-6	16.0	0.50 ± 0.05	0.5 ± 0.1 (0.3)	0.50 ± 0.07	0.12 ± 0.04
ZnO-7	5.6	0.64 ± 0.01	3.2 ± 0.4 (2.9)	0.49 ± 0.01	1.0 ± 0.1
ZnO-8	5.8	0.63 ± 0.02	3.5 ± 0.4 (2.7)	0.49 ± 0.04	1.1 ± 0.1

[a]Average performance (mean values) has been calculated for 4 devices. J_{sc} values in brackets were estimated from IPCE.

and photovoltaic transient measurements to study the charge transport and collection in the samples. Generally, improved performance of DSSCs is commonly attributed to the improved dye adsorption due to optimized morphology[17] or optimized layer thickness and dye loading time,[20] as well as fast electron transport.[17] Increased electron lifetime was also identified as one of the factors contributing to the improved performance of ZnO-based DSSCs.[18] However, it was also shown that high efficiencies can be achieved when the electron transfer time is much shorter than the electron lifetime.[21] Therefore, cells with shorter electron lifetime could have higher efficiency as long as the electron transfer time is very short.[21] Consequently, it is necessary to study the charge transport and collection in detail to improve our understanding of the influence of these factors on the overall cell performance. The obtained results from EIS measurements and photovoltage and photocurrent transient measurements are shown in Figure 7 and summarized in Table 3.

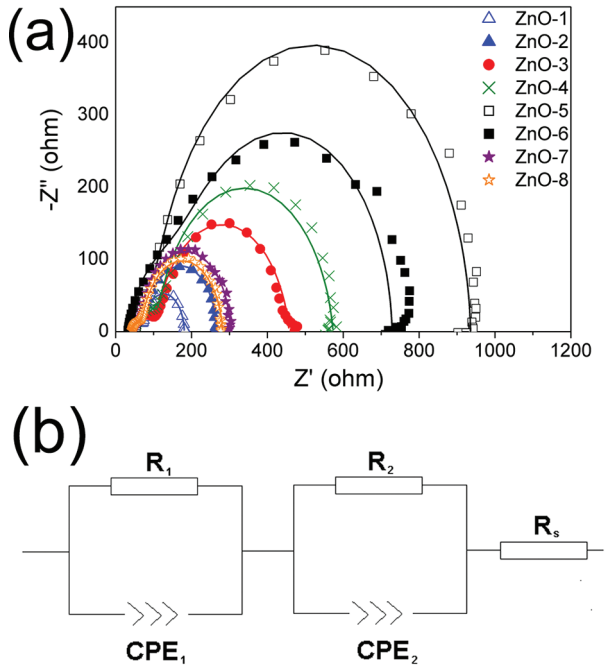

Figure 7. (a) Nyquist plot of DSSCs prepared using different ZnO nanoparticles for the active layer and (b) the equivalent circuit used for fitting.

The EIS spectra shown in Figure 7 exhibit a characteristic two loop form.[21,30,34] The smaller loop at high frequencies (in kHz range) represents the charge transfer resistance at Pt electrode/electrolyte interface.[34] The larger loop at lower frequencies (10−100 Hz range) represents the charge transfer process at the ZnO/dye/electrolyte interface.[34]

The electron lifetimes from the EIS measurements were calculated from parameters obtained by fitting the impedance data using an appropriate equivalent circuit model which is also shown in Figure 7.[21,30] In the model, R_s is the contact resistance,[21] the constant phase elements (used for better fitting instead of the usual capacitance[21,31]) are described with $CPE_i = 1/T_i(j\omega)^{Pi}$, where $0 < P_i < 1$, for $i = 1, 2$.[21] R_i $(i = 1, 2)$ represented the charge transfer and recombination process for each of the DSSC electrodes. The dispersion of the capacitance of ZnO electrodes could be calculated as:[21,32] $C_2 = (R_2^{1-P2}T_2)^{1/P2}$ and the corresponding electron lifetime as:[30,33] $\tau_{eEIS} = R_2C_2$. The electron lifetimes obtained from the transient photovoltage measurements and the EIS measurements show similar trends, although the values obtained from the transient photovoltage measurements are lower compared to those obtained from the EIS measurements, similar to previous reports.[38] Different local concentrations of I_3^- were also proposed as an explanation for the observed differences in the electron lifetimes obtained by the two techniques.[38] In principle, these two techniques should give an equivalent result.[33] However, we have found that the obtained electron lifetime from transient photovoltage measurements exhibits some degree of dependence on the frequency of the red bias light (~100 ms difference for the range ~0.1 to 3 Hz for ZnO-1). The origin of this dependence is not fully clear and it may depend on the surface states present in the particles. It has been shown that when the charge transfer is dominated by the surface states, the free electron lifetime can depend on the bias.[33] Furthermore, experimental artifacts could affect the results of the two techniques, for example, contributions to the capacitance by the counter electrode and electrolyte diffusion, or the capacitance is dominated by the depletion region at the surface of ZnO and the time constant for the lower frequency recombination arc does not correspond to the electron lifetime.[33]

It is well-known that for an optimal photovoltaic performance it is necessary to have fast electron injection, high dye adsorption, long electron lifetime, and short electron transport time. While the nanoparticle properties exhibit complex relationship with these parameters and consequently photovoltaic performance, we can clearly observe that a high concentration of nonradiative defects at the surface of nanoparticles is a nanoparticle property which is detrimental to photovoltaic performance. From the obtained results for active layer parameters, we can conclude that the long electron lifetime is the most significant factor determining the performance, in agreement with

Table 3. Summary of EIS and Transient Measurements Parameters[a]

	T_1	P_1	R_1 (Ω)	T_2	P_2	R_2 (Ω)	R_s (Ω)	τ_{eEIS} (ms)	τ_e (ms)	τ_{trans} (ms)
ZnO-1	4.79×10^{-5}	0.86	34.07	6.74×10^{-4}	0.98	107.2	39.45	68.5	536.7	354.8
ZnO-2	4.38×10^{-5}	0.87	42.46	1.31×10^{-4}	0.98	182.7	40.95	22.2	37.9	133.7
ZnO-3	2.35×10^{-5}	0.94	55.73	9.58×10^{-4}	0.89	354.9	49.65	297.7	1056.3	337.4
ZnO-4	2.17×10^{-5}	0.97	58.4	3.85×10^{-4}	0.90	464.7	50.16	147.8	123.9	270.7
ZnO-5	4.42×10^{-5}	0.88	56.6	4.18×10^{-5}	0.97	826.3	52.91	31.1	155.1	60.1
ZnO-6	3.62×10^{-5}	0.86	163.5	6.24×10^{-5}	0.98	532.1	33.25	31.0	297.0	109.0
ZnO-7	5.52×10^{-5}	0.87	23.58	1.62×10^{-4}	0.96	235.4	44.53	33.3	164.0	88.4
ZnO-8	4.37×10^{-5}	0.89	26.71	2.05×10^{-4}	0.95	211.2	43.75	36.7	133.0	128.3

[a] τ_{trans} denotes electron transport time, τ_e denotes electron lifetime obtained from transient photovoltage measurements, τ_{eEIS} denotes electron lifetime obtained from EIS measurements, whereas T_1, P_1, R_1, T_2, P_2, R_2, and R_s denote fitting parameters for the equivalent circuit for EIS.

a previous report,[18] although similar to PL intensity it is not a sufficient determining factor to guarantee better performance. Although it was reported that a shorter electron lifetime can result in higher efficiency if the transport time is very short,[21] in our samples we do not have any which satisfy this condition. Furthermore, we can observe that the long electron lifetimes (from transient photovoltage measurements) are associated with the samples exhibiting orange-red defect emission. Possible reasons for this would be that defects responsible for orange-red emission are likely to be bulk not surface defects, which could affect the recombination losses of the electrons in ZnO. Exact nature of these defects requires further study. In any case, we can conclude that lower concentrations of nonradiative defects are desirable, and that orange-red emitting defects are desirable to achieve improved performance of ZnO DSSCs. The performances obtained here would likely be improved by optimization of the layer thickness, dye loading, and the introduction of a scattering layer. Furthermore, it is also possible that performance of some of the samples which tend to aggregate could be improved by the employment of more vigorous paste preparation procedures to improve uniformity (high power sonication, mechanical stirring).

4. CONCLUSIONS

We have investigated the influence of the optical properties of ZnO nanoparticles on the DSSC performance. As expected, for optimal performance, it is necessary to compromise between fast electron transport, high dye adsorption, long electron lifetime, and fast electron injection. However, we also found that the presence of orange-red emitting defects is associated with higher short circuit current density and lower open circuit voltage and fill factor compared to green emission, whereas a high concentration of nonradiative defects (resulting in a weak photoluminescence of ZnO nanoparticles) was detrimental to photovoltaic performance and also associated with significant nanoparticle aggregation and lower ratio of lattice oxygen to loosely bound surface oxygen. The relationship between other performance parameters and nanoparticle properties is complex and requires further study.

■ ASSOCIATED CONTENT

Ⓢ Supporting Information

XPS results and PL spectra for different annealing conditions. This material is available free of charge via the Internet at http://pubs.acs.org/.

■ AUTHOR INFORMATION

Corresponding Author

*Tel: +852 2859 7946. Fax: +852 2559 9152. E-mail: dalek@hku.hk.

Notes

The authors declare no competing financial interest.

■ ACKNOWLEDGMENTS

Financial support from the project RGC CRF CityU6/CRF/08 and the Strategic Research Theme, University Development Fund, and Small Project Funding of the University of Hong Kong is acknowledged. The authors thank Prof. K. Y. Chan, the University of Hong Kong, and Prof. Raymond Wong, Hong Kong Baptist University, for BET surface area measurements, and Materials Characterization and Preparation Facility, Hong Kong University of Science and Technology, for XPS measurements.

■ REFERENCES

(1) Boucharef, M.; Bin, C. D.; Boumaza, M. S.; Colas, M.; Snaith, H. J.; Ratier, B.; Boucle, J. *Nanotechnology* **2010**, *21* (1−12), 205203.
(2) Wu, C. T.; Liao, W. P.; Wu, J. J. *J. Mater. Chem.* **2011**, *21*, 2871−2876.
(3) Guerin, V. M.; Magne, C.; Pauporte, T.; Bahers, T. L.; Rathousky, J. *ACS Appl. Mater. Interfaces* **2010**, *2*, 3677−3685.
(4) Jimenez-Cadena, G.; Comini, E.; Ferroni, M.; Vomiero, A.; Sberveglieri, G. *Mater. Chem. Phys.* **2010**, *124*, 694−698.
(5) Horiuchi, H.; Katoh, R.; Hara, K.; Yanagida, M.; Murata, S.; Arakawa, H.; Tachiya, M. *J. Phys. Chem. B* **2003**, *107*, 2570−2574.
(6) Ku, C. H.; Wu, J. J. *Appl. Phys. Lett.* **2007**, *91* (1−3), 093117.
(7) Quintana, M.; Edvinsson, T.; Hagfeldt, A.; Boschloo, G. *J. Phys. Chem. C* **2007**, *111*, 1035−1041.
(8) Bacsa, R. R.; Dexpert-Ghys, J.; Verelst, M.; Falqui, A.; Machado, B.; Bacsa, W. S.; Chen, P.; Zakeeruddin, S. M.; Graetzel, M.; Serp, P. *Adv. Funct. Mater.* **2009**, *19*, 875−886.
(9) Hsu, Y. F.; Xi, Y. Y.; Djurišić, A. B.; Chan, W. K. *Appl. Phys. Lett.* **2008**, *92* (1−3), 133507.
(10) Gao, H. M.; Fang, G. J.; Wang, M. J.; Liu, N. S.; Yuan, L. Y.; Li, C.; Ai, L.; Zhang, J.; Zhou, C. H.; Wu, S. J.; Zhao, X. Z. *Mater. Res. Bull.* **2008**, *43*, 3345−3351.
(11) Seow, Z. L. S.; Wong, A. S. W.; Thavasi, V.; Jose, R.; Ramakrishna, S.; Ho, G. W. *Nanotechnology* **2009**, *20* (1−6), 045604.
(12) Yodyingyong, S.; Zhang, Q. F.; Park, K.; Dandeneau, C. S.; Zhou, X. Y.; Triampo, D.; Cao, G. Z. *Appl. Phys. Lett.* **2010**, *96* (1−3), 073115.
(13) Zhang, Y. Z.; Wu, L. H.; Liu, Y. P.; Xie, E. Q. *J. Phys. D: Appl. Phys.* **2009**, *42* (1−6), 085105.
(14) Lupan, O.; Guerin, V. M.; Tiginyanu, I. M.; Ursaki, V. V.; Chow, L.; Heinrich, H.; Pauporte, T. *J. Photochem. Photobiol., A* **2010**, *211*, 65−73.
(15) Cheng, H. M.; Hsieh, W. F. *Nanotechnology* **2010**, *21* (1−8), 485202.
(16) Law, M.; Greene, L. E.; Johnson, J. C.; Saykally, R.; Yang, P. D. *Nat. Mater.* **2005**, *4*, 455−459.
(17) Dong, H. P.; Wang, L. D.; Gao, R.; Ma, B. B.; Qiu, Y. *J. Mater. Chem.* **2011**, *21*, 19389−19394.
(18) Lai, Y. H.; Lin, C. Y.; Chen, H. W.; Chen, J. G.; Kung, C. W.; Vittal, R.; Ho, K. C. *J. Mater. Chem.* **2010**, *20*, 9379−9385.
(19) Marczak, R.; Werner, F.; Ahmad, R.; Lobaz, V.; Guldi, D. M.; Peukert, W. *Langmuir* **2011**, *27*, 3920−3929.
(20) Saito, M; Fujihara, S. *Energy Environ. Sci.* **2008**, *1*, 280−283.
(21) Guerin, V. M.; Magne, C.; Pauporté, Th.; Le Bahers, T.; Rathousky, J. *ACS Appl. Mater. Interfaces* **2010**, *2*, 3677−3685.
(22) Wu, J. J.; Chen, G. R.; Yang, H. H.; Ku, C. H.; Lai, J. Y. *Appl. Phys. Lett.* **2007**, *90* (1−3), 213109.
(23) Wu, C. T.; Wu, J. J. *J. Mater. Chem.* **2011**, *21*, 13605−13610.
(24) Guo, M. Y.; Ng, A. M. C.; Liu, F. Z.; Djurišić, A. B.; Chan, W. K.; Su, H. M.; Wong, K. S. *J. Phys. Chem. C* **2011**, *115*, 11095−11101.
(25) Ito, S.; Murakami, T. N.; Comte, P.; Liska, P.; Grätzel, C.; Zakeerudin, M. K.; Grätzel, M. *Thin Solid Films* **2008**, *516*, 4613−4619.
(26) Koops, S. E.; Durrant, J. R. *Inorg. Chim. Acta* **2008**, *361*, 663−670.
(27) Yoshihara, T.; Katoh, R.; Furube, A.; Murai, M.; Tamaki, Y.; Hara, K.; Murata, S.; Arakawa, H.; Tachiya, M. *J. Phys. Chem. B* **2004**, *108*, 2643−2647.
(28) Green, A. N. M.; Palomares, E.; Jaque, S. A.; Kroon, J. M.; Durrant, J. R. *J. Phys. Chem. B* **2005**, *109*, 12525−12533.
(29) Lu, L. L.; Li, R. J.; Fan, K.; Peng, T. Y. *Solar Energy* **2010**, *84*, 844−853.
(30) Sudhagar, P.; Kumar, R. S.; Jung, J. H.; Cho, W. H.; Sathyamoorthy, R.; Won, J.; Kang, Y. S. *Mater. Res. Bull.* **2011**, *46*, 1473−1479.

(31) Jorcin, J. B.; Orazem, M. E.; Pébère, N.; Tribollet, B. *Electrochim. Acta* **2006**, *51*, 1473−1479.
(32) Pauporté, T.; Finne, J. *J. Appl. Electrochem.* **2006**, *36*, 33−41.
(33) Bisquert, J.; Fabregat-Santiago, F.; Mora-Seró, I.; Garcia-Belmonte, G.; Giménez, S. *J. Phys. Chem. C* **2009**, *113*, 17278−17290.
(34) Chen, H.-W.; Lin, C.-Y.; Lai, Y.-H.; Chen, J.-G.; Wang, C.-C.; Hu, C.-W.; Hsu, C.-Y.; Vittal, R.; Ho, K.-C. *J. Power Sources* **2011**, *196*, 4859.
(35) Wang, Q.; Moser, J.-E.; Grätzel, M. *J. Phys. Chem. B* **2005**, *109*, 14945−14953.
(36) Wang, X. X.; Karanjit, S.; Zhang, L. F.; Fong, H.; Qiao, Q. Q.; Zhu, Z. T. *Appl. Phys. Lett.* **2011**, *98* (1−3), 082114.
(37) Yip, C. T.; Mak, C. S. K.; Djurišić, A. B.; Hsu, Y. F.; Chan, W. K. *Appl. Phys. A: Mater. Sci. Process.* **2008**, *92*, 589−593.
(38) Kuang, D. B.; Klein, C.; Zhang, Z. P.; Ito, S.; Moser, J. E.; Zakeerudin, S. M.; Grätzel, M. *Small* **2007**, *3*, 2094−2102.
(39) Chen, X. Y.; Yip, C. T.; Fung, M. K.; Djurišić, A. B.; Chan, W. K. *Appl. Phys. A: Mater. Sci. Process.* **2010**, *100*, 15−19.
(40) Ogunsola, O.; Park, J.; Lee, G.; Ehrman, S. *J. Mater. Res.* **2006**, *21*, 1738−1746.
(41) Ali, M.; Winterer, M. *Chem. Mater.* **2010**, *22*, 85−91.
(42) Tam, K. H.; Cheung, C. K.; Leung, Y. H.; Djurišić, A. B.; Ling, C. C.; Beling, C. D.; Fung, S.; Kwok, W. M.; Chan, W. K.; Phillips, D. L.; Ding, L.; Ge, W. K. *J. Phys. Chem. B* **2006**, *110*, 20865−20871.
(43) Lu, Y. F.; Ni, H. Q.; Mai, Z. H.; Ren, Z. M. *J. Appl. Phys.* **2000**, *88*, 498−502.
(44) Djurišić, A. B.; Ng, A. M. C.; Chen, X. Y. *Prog. Quantum Electron.* **2010**, *34*, 191−259.
(45) Djurišić, A. B.; Leung, Y. H.; Tam, K. H.; Hsu, Y. F.; Ding, L.; Ge, W. K.; Zhong, Y. C.; Wong, K. S.; Chan, W. K.; Tam, H. L.; Cheah, K. W.; Kwok, W. M.; Phillips, D. L. *Nanotechnology* **2007**, *18* (1−8), 095702.